Double Mutant Studies Identify Electrostatic Interactions That Are Important for Docking Cytochrome c_2 onto the Bacterial Reaction Center†

M. Tetreault,‡ M. Cusanovich,§ T. Meyer,§ H. Axelrod,‡ and M. Y. Okamura*,‡

Department of Physics 0319, 9500 Gilman Drive, University of California at San Diego, La Jolla, California 92093, and Department of Biochemistry and Molecular Biophysics, University of Arizona, Tucson, Arizona 85721

Received November 13, 2001; Revised Manuscript Received March 6, 2002

ABSTRACT: Cytochrome c_2 (cyt) is the mobile electron donor to the reaction center (RC) in photosynthetic bacteria. The electrostatic interactions involved in the dynamics of docking of cyt onto the RC were examined by double mutant studies of the rates of electron transfer between six modified *Rhodobacter sphaeroides* RCs in which negatively charged acid residues were replaced with Lys and five modified *Rhodobacter capsulatus* Cyt c_2 molecules in which positively charged Lys residues were replaced with Glu. We measured the second-order rate constant, k_2, for electron transfer from the reduced cyt to the oxidized primary donor on the RC, which reflects the energy of the transition state for the formation of the active electron transfer complex. Strong interactions were found between Lys C99 and Asp M184/Glu M95, and between Lys C54 and Asp L261/Asp L257. The interacting residues were found to be located close to each other in the recently determined crystal structure of the cyt−RC complex [Axelrod, H., et al. (2002) *J. Mol. Biol.* (in press)]. The interaction energies were approximately inversely proportional to the distances between charges. These results support earlier suggestions [Tetreault, M., et al. (2001) *Biochemistry 40*, 8452−8462] that the structure of the transition state in solution resembles the structure of the cyt−RC complex in the cocrystal and indicate that specific electrostatic interactions facilitate docking of the cyt onto the RC in a configuration optimized for both binding and electron transfer. The specific interaction between Asp M184 and Lys C99 may help to nucleate short-range hydrophobic contacts.

Electrostatic interactions are important in the docking process of proteins that are associated with intermolecular electron transfer reactions in photosynthesis and respiration (*1*). This work deals with the electrostatic interactions between the photosynthetic reaction center (RC)[1] (*2*) and its electron donor cytochrome c_2 (cyt) (*3*). In photosynthetic membranes, the RC initiates light-induced electron transfer from a primary donor species, D, a bacteriochlorophyll dimer, through a series of electron acceptors, bacteriochlorophyll, bacteriopheophytin, and ubiquinone (Q_A), to reduce a bound quinone Q_B. The fully reduced Q_B dissociates from the RC and transfers its electrons to the cytochrome bc_1 complex, pumping protons across the membrane. The reduced cytochrome bc_1 complex transfers electrons to the RC by means of the water soluble cytochrome c_2. The reduction of the oxidized donor D^+ by the cytochrome c_2 is the reaction that completes the photosynthetic electron transfer cycle.

The light-induced electron transfer reactions between isolated cyt c_2 and the RC have been extensively studied (*4*−*9*). See ref *3* for a review. The reaction scheme for the RC−cytochrome interaction is shown below.

$$\begin{array}{lcc} & K_B = 1/K_D & \\ \text{Dark} & \mathrm{cyt}^{2+} + \mathrm{DQ} \rightleftharpoons \mathrm{cyt}^{2+}\text{:}\mathrm{DQ} & (1) \\ & \downarrow h\nu \qquad\qquad \downarrow h\nu & \\ & \overset{k_2}{\rightleftharpoons} \qquad \overset{k_e}{\longrightarrow} & \\ \text{After laser flash} & \mathrm{cyt}^{2+} + \mathrm{D}^+\mathrm{Q}^- \rightleftharpoons \mathrm{cyt}^{2+}\text{:}\mathrm{D}^+\mathrm{Q}^- \longrightarrow \mathrm{cyt}^{3+}\text{:}\mathrm{D}\,\mathrm{Q}^- & \end{array}$$

The top line indicates the RC in its neutral ground state (DQ) in the dark, reversibly binding a cyt with a dissociation constant K_D of 0.3 μM (pH 7.5, 10 mM ionic strength) (*9*). The reaction after photooxidation of the primary donor by a laser pulse is shown on the second line in eq 1. Two phases of donor reduction are observed, a fast first-order phase with a rate constant k_e of 1.1×10^6 s^{-1} due to cytochrome bound on the surface of the RC and a slow second-order phase, k_2, due to the RC reacting with free cyt (*9*). The amplitude of the fast phase depends on the concentration of cyt, but the rate constant k_e is independent of concentration. The rate of the slow phase depends on cyt concentration, giving a second-order rate constant close to the diffusion limit [$k_2 \approx 1.6 \times 10^9$ s^{-1} M^{-1} (pH 7.5, 10 mM ionic strength) (*9*)]. The first-order rate constant is dependent on the driving force for electron transfer, indicating a rate-limiting electron transfer mechanism; the second-order rate constant is independent of the driving force, indicating that the rate-limiting step involves an association process leading to the complex active in electron transfer (*10*). In this work, we deal with

† The work was supported by NSF Grant MCB99-74568, NIH Grant GM 13191, and NIH Grant GM21277.

* To whom correspondence should be addressed. Phone: (858) 534-2506. Fax: (858) 822-0007. E-mail: mokamura@ucsd.edu.

‡ University of California at San Diego.

§ University of Arizona.

[1] Abbreviations: RC, reaction center; cyt, cytochrome; k_2, second-order rate constant; K_D, dissociation constant; Q_o, 2,3-dimethoxy-5-methyl-1,4-benzoquinone.

10.1021/bi012053e CCC: $22.00
Published on Web 04/16/2002

Table 1: Dissociation Constants, K_D, and Second-Order Rate Constants, k_2, for the Reaction of Cytochromes c_2 from *Rb. capsulatus* and *Rb. sphaeroides* with Native and Mutant RCs from *Rb. sphaeroides*[a]

	K_D (caps) (μM)	K_D (sph) (μM)	k_2 (caps) ($\times 10^8$ s^{-1} M^{-1})	k_2 (sph) ($\times 10^8$ s^{-1} M^{-1})
native	0.5	0.34	16	16.5
DK (L257)	4	7	7	7
EK (M95)	49	41	3.8	2
DK (L155)	4.3	5.2	7.3	7
DK (M292)	30	11.1	7	5.3
DK (L261)	49	55	3	3.5
DK (M184)	100	250	3	1

[a] Conditions: 1 μM RC, 10 mM Hepes (pH 7.5), 0.04% dodecyl β-maltoside, 0.1 mM EDTA, and 23 °C. The experimental error is ±15% unless otherwise stated.

the interaction between the RC from *Rhodobacter sphaeroides* and the cyt c_2 from *Rhodobacter capsulatus*, a system for which the mutagenesis has been worked out (*11*). The cyt from *Rb. capsulatus* has reaction properties very similar to those of *Rb. sphaeroides*, with the following values: $k_e = 1.4 \times 10^6$ s^{-1}, $K_D = 0.5 \times 10^{-6}$ M^{-1}, and $k_2 = 1.6 \times 10^9$ s^{-1} M^{-1} (*12*) (Table 1).

An important question concerns the structure of the cyt−RC complex in the bound state as well as the structure and dynamics of the cyt−RC complex in the transition state. The involvement of electrostatic interactions in the binding and electron transfer was shown by the ionic strength dependence of the dissociation constant and second-order rate constant (*4*, *7*). The involvement of acidic residues on the RC and basic residues on the cyt was shown by chemical modification (*13*), cross-linking (*14*, *15*), site-directed mutation of negatively charged residues on the RC from *Rb. sphaeroides* (*9*), and mutation of positively charged residues on the cyt c_2 from *Rb. capsulatus* (*11*). Experiments bearing on the structure of the cyt−RC complex have been performed using electrostatic modeling (*16*−*19*), light-induced dichroism measurements (*20*), and X-ray crystallography (*18*, *21*).

The structures of the interaction surfaces of the cyt and RC are shown in Figure 1. The structures of cyt c_2 from *Rb. capsulatus* and *Rb. sphaeroides* show the solvent-exposed heme edge (orange) surrounded by positively charged Lys residues (blue) (Figure 1a,b). The surface of the RC contains a central solvent-exposed Tyr L162 (green), located directly above the bacteriochlorophyll dimer, surrounded by negatively charged Asp and Glu residues (red) (Figure 1c). Tyr L162 has been proposed to be the docking surface for the heme edge in most models for the complex by analogy with the structure of the *Rhodopseudomonas viridis* (now called *Blastochloris viridis*) RC that contains a nondissociating cytochrome. The involvement of Tyr L162 in the docking of cyt c_2 and the RC was shown by large changes (2 orders of magnitude) in the rate of electron transfer due to mutation of Tyr L162 in *Rb. sphaeroides* RCs (*22*). This change can be attributed to a change in the docking of the complex, since only small changes in the electron transfer rate (typically, 2-fold) were observed for mutations of Tyr L162 in *Rps. viridis* RCs, where the cyt is permanently bound to the RC (*23*). Recently, a high-resolution X-ray crystal structure of a co-crystal of cyt and the RC from *Rb. sphaeroides* was obtained (*21*). It shows the heme edge in contact with Tyr L162, as in the *Rps. viridis* structure, in position for fast

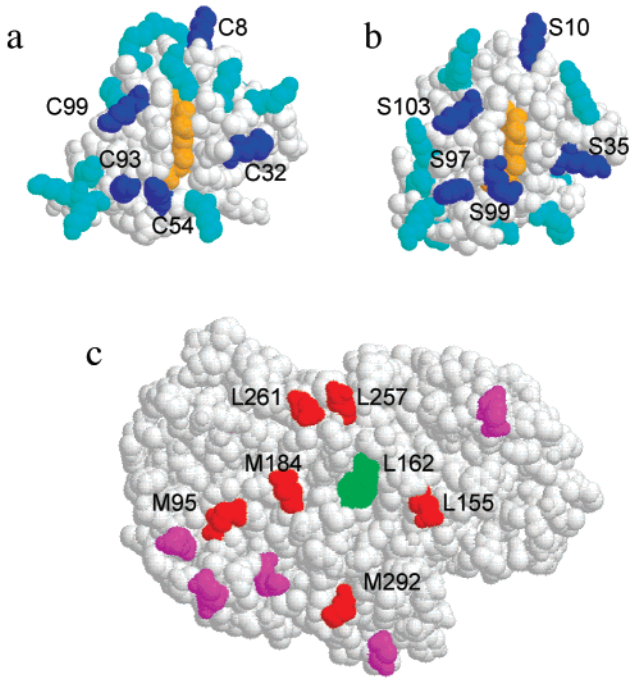

FIGURE 1: Views of the interaction surfaces of (a) cyt c_2 from *Rb. capsulatus*, (b) cyt c_2 from *Rb. sphaeroides*, and (c) the RC from *Rb. sphaeroides*. The mutated Lys residues on the cyt from *Rb. capsulatus* (labeled C8, C32, C54, C93, and C99) and structurally homologous residues in the cyt from *Rb. sphaeroides* (labeled S10, S35, S99, S97, and S103, respectively) are shown in blue. The mutated acidic residues on the RC are shown in red. The charged residues that were not mutated are shown in light blue on the cyt and light red on the RC. The proposed electron transfer contact groups, the heme (orange) on the cyt and Tyr L162 (green), are shown.

electron transfer. In addition, the binding interface between the cyt and RC shows a short-range binding domain with hydrophobic, hydrogen bonding, and cation−pi interactions that orient the heme on Tyr L162, and a long-range electrostatic binding domain having complementary charged residues on cyt and the RC in the proximity, but not in salt-bridged configurations.

In the study presented here, we address the question of the dynamics of the docking of the cyt onto the RC surface prior to electron transfer, i.e., the mechanism of the second-order electron transfer reaction. Early discussions of the electrostatic docking emphasized the role of specific ion pair interactions in forming the cyt−RC complex and recognized the importance of the cluster of acidic residues surrounding Asp M184 on the RC (*16*−*18*). Subsequent discussions have emphasized the overlap of diffuse complementary potential energy surfaces on the RC and the cyt (*12*, *19*) rather than the interaction between specific salt-bridged residues. Recent mutational studies (*9*) as well as the cocrystal structure (*21*) have shown that in addition to long-range electrostatic interactions, short-range interactions are important in forming the cyt−RC complex.

A mechanism for the reaction between cyt and the RC (*9*) is shown schematically in eq 2. As the cyt in solution approaches the RC, they form an encounter complex (cyt^{2+}−RC) that is stabilized by long-range electrostatic forces between the positively charged residues on the cyt surface and negatively charged residues on the RC surface. The cyt moves within the encounter complex until it reaches the

transition state $(cyt^{2+}-RC)^{\ddagger}$. The transition state is the conformation at the top of the energy barrier that leads directly to the active state in electron transfer, $(cyt^{2+}-RC)^*$. This is followed by the electron transfer reaction with the rate consant k_e, resulting in the oxidation of the cyt and reduction of the bacteriochlorophyll dimer in the RC, $(cyt^{3+}-RC^-)^*$

$$cyt^{2+} + RC \leftrightarrow (cyt^{2+}-RC) \leftrightarrow (cyt^{2+}-RC)^{\ddagger} \rightarrow (cyt^{2+}-RC)^* \xrightarrow{k_e} (cyt^{3+}-RC^-)^* \quad (2)$$

The correlation between the second-order rate constant and binding constants of different mutant RCs showed that mutations that result in changes to the energy of the final state, $\Delta\Delta G^\circ$, also produce changes to the energy of the transition state, $\Delta\Delta G^{\circ\ddagger}$ (*9*). The changes in these energies were related by a constant, α, obtained from the slope of the log plot of the second-order rate constant and binding constant.

$$\Delta\Delta G^{\circ\ddagger} = \alpha\Delta\Delta G^\circ \quad (3)$$

The relatively constant value for α of 0.4 ± 0.06 suggested that the transition state partially resembles the final state. The low value of α could be explained by a model in which the cyt and RC in the transition state were in the same configuration as in the final state but moved away from each other with the distances between charges increased by a factor of $1/\alpha$ ($\sim$2-fold), thereby decreasing the electrostatic interaction energies in the transition state.

The picture of the transition state described above was derived from studies in which changes in transition state and binding energies were obtained due to single mutations on the RC. In this work, we ask what specific interactions between charged residues steer the cyt into the proper state for electron transfer, i.e., what specific interactions are important in the transition state. To answer this question, we studied the effects of mutations to both the RC and the cyt on the second-order rate constant, k_2. This method of double mutant reactions has been used to study electrostatic interactions between mutated residues in other proteins (*24*−*28*). Single mutations were introduced into RCs from *Rb. sphaeroides* by replacing six acidic residues (Asp L155, Asp L257, Asp L261, Glu M95, Asp M184, and Asp M292) with Lys (*9*) (see Figure 1c). In addition, single mutations were introduced into cyt c_2 from *Rb. capsulatus* by replacing five Lys residues (C8, C32, C54, C93, and C99) with Glu (*11*) (see Figure 1a). These residues were chosen because there are structurally similar residues on the cyt c_2 from *Rb. sphaeroides*. The positions of the corresponding residues are S10, S35, S99, S97, and S103 (see Figure 1b). It is interesting to note that residue Lys C54 from *Rb. capsulatus* is structurally analogous to residue Lys S99 in *Rb. sphaeroides* that is a long distance away in the sequence. The energy of interaction between specific mutated sites on the cyt and RC was obtained by measuring the changes to rate constants k_2, for reactions involving double mutants (mutant cyt and mutant RC) and single mutants. The energy of interaction between mutated sites is the difference between the transition state energy in the reaction involving double mutants and the sum of the changes in transition state energy due to single mutations. The results provide evidence for interaction between specific charged residues at the interface of the cyt−RC complex that contribute to the docking of the two proteins for electron transfer. A preliminary report of this work has been presented (*29*).

MATERIALS AND METHODS

Sample Preparation. The construction of RC mutants by site-directed mutagenesis was performed as previously described (*9*). Cytochrome mutants were prepared using the Clontech TRANSFORMER site-directed mutagenesis kit with the *Rb. capsulatus Bgl*II/*Sal*I fragment, which contains the *cycA* gene (*30*), inserted into the *Hin*dIII/*Kpn*I site of pUC19 as a template. After mutant DNA sequence verification, this *Hin*dIII/*Kpn*I fragment was inserted into the same restriction sites of pRK415 (10.6 kB, Tet^R) (*31*) and transformed into *Escherichia coli* S17-1 which was then used for biparental mating with *Rb. capsulatus* MT-G4/S4 [*crt*D121 Δ_1 (*cyc*A::*kan*)Rif^R] (*30*), a kanamycin resistant cytochrome c_2 deletion mutant. The parental cross was accomplished by mixing equal volumes of cell pellets from approximately 3 mL of liquid culture on an RCVB (*32*) plate, incubating overnight at 30 °C, and then replating the colonies on selective RCVB, 2.5 μg/mL tetracycline, and 25 μg/mL kanamycin. Cells were eventually cultured anaerobically in a 20 L fermenter, in which the medium was titrated with malic acid to increase the cell yield.

Cytochrome c_2 was purified from recombinant cells of *Rb. capsulatus* by the following method. Cell-free extracts were batch-adsorbed and eluted from DEAE-cellulose, desalted on Sephadex G25, adjusted to pH 8 in 10 mM Tris-HCl, and chromatographed on DEAE-Sepharose CL-6B (Pharmacia) using a 0 to 250 mM NaCl linear gradient. Samples were assayed for purity by measuring the ratio of absorbance at 280 nm to that at 412 nm. If further purification was required, the cytochrome was chromatographed on hydroxyapatite (Biorad Macro-Prep Type I, 40 μm) using a 5 to 200 mM potassium phosphate linear gradient in 100 mM NaCl (pH 7). The cyt stock solution was dialyzed against 10 mM Hepes buffer (pH 7.5). The cyt concentration was determined using an extinction coefficient ϵ_{550}(reduced) of 30.8 cm^{-1} mM^{-1} (*33*). The mutated RCs were obtained from aerobically grown bacteria and purified as described previously (*34*).

Electron Transfer Measurements. The kinetic measurements were taken as described (*9*) using transient absorption spectroscopy. The reactions were initiated by a laser pulse from a dye laser (Phase-R, $\lambda = 590$ nm, $\tau = 300$ ns). Absorption changes accompanying electron transfer were monitored at either 595 or 865 nm using a modified Cary 14 spectrophotometer (Varian). Flash-induced absorbance data were collected on a Le Croy oscilloscope and transferred to a computer for analysis. All measurements were performed at 23 °C in a buffer of 10 mM Hepes, 0.04% β-D-maltoside, and 0.1 mM EDTA (pH 7.5). Prior to kinetic measurements, 0.1 mM Q_0 and 0.1 mM Q_0H_2 were added as a redox buffer, ensuring that cyt c_2 was fully reduced before each laser flash.

The second-order rate constants were determined on samples having a RC concentration of 1 μM by monitoring the slow phase in the re-reduction of the RC due to kinetics of association of cyt c_2 and the RC. The slow phase was monitored in samples where the concentration of free cyt

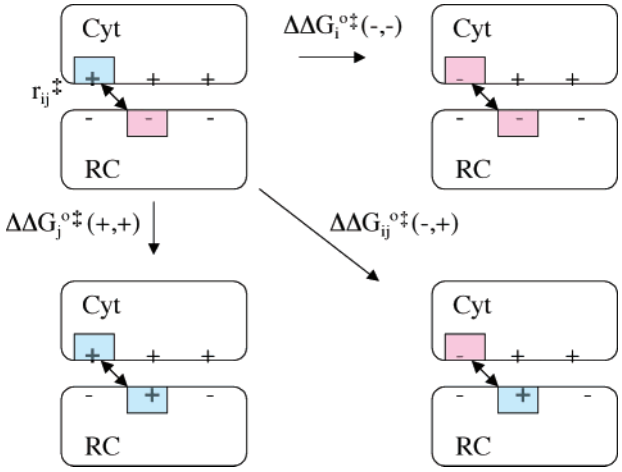

FIGURE 2: Interactions in cyt−RC transition state complexes having different charges at residue *i* on the cyt and *j* on the RC. The energy $\Delta\Delta G_{ij}^{\circ\ddagger}$(int) of the interaction between mutated sites in the double mutant complex is the difference between the change in free energy for forming the complex having two mutations, $\Delta\Delta G_{ij}^{\circ\ddagger}(-,+)$ (diagonal arrow), and the sum of the changes due to the single mutations, $\Delta\Delta G_{ij}^{\circ\ddagger}(+,+) + \Delta\Delta G_{ij}^{\circ\ddagger}(-,-)$ (horizontal and vertical arrows). $\Delta\Delta G_{ij}^{\circ\ddagger}$(int) is assumed to be proportional to the magnitude of the electrostatic interaction between the charges on residues *i* and *j* in the transition state of native RCs.

c_2, [cyt^{2+}], was large compared to the concentration of the unbound RC, [RC^+], so that the reaction, $d[RC^+]/dt = k_2[cyt^{2+}][RC^+]$, is pseudo-first-order. The pseudo-first-order rate constant, k_{obs}, was plotted versus free cyt c_2 concentration to obtain the second-order rate constant. The dissociation constant K_D was determined by monitoring the fraction of RCs having a fast ($\tau_e = 1$ μs) component, i.e., the fraction of RCs having a bound cyt, as a function of cyt concentration (*9*).

Analysis of Data. The double mutant analysis can be used to obtain information about interactions between residues in the transition state leading to the active cyt−RC complex by measuring the changes in k_2 due to single or double mutations (*24*−*27*). The transition state complexes for the reactions between cyt−RC complexes containing different combinations of charges at the mutated residues are shown in Figure 2. In the native system, the complex is stabilized by opposite charges on the cyt and RC surfaces. The mutation of a positively to negatively charged residue *i* on the cyt and a negatively to positively charged residue *j* on the RC results in increases in the transition state energies, $\Delta\Delta G_i^{\circ\ddagger}(-,-)$ and $\Delta\Delta G_j^{\circ\ddagger}(+,+)$, respectively. The mutation of both residues results in a change in energy of $\Delta\Delta G_{ij}^{\circ\ddagger}(-,+)$ which may be smaller than the sum of the single mutant changes if there is an interaction between the mutation sites. The interaction energy $\Delta\Delta G_{ij}^{\circ\ddagger}$(int) can be defined as the difference between the change in the energy of formation of the complex having two mutations and the sum of energies of formation of the complexes having single mutations.

$$\Delta\Delta G_{ij}^{\circ\ddagger}(\text{int}) = \Delta\Delta G_{ij}^{\circ\ddagger}(-,+) - [\Delta\Delta G_i^{\circ\ddagger}(-,-) + \Delta\Delta G_j^{\circ\ddagger}(+,+)] \quad (4)$$

where *i* and *j* refer to the mutated residues on the cyt and RC, respectively. The interaction energy can be obtained from the measured values of the second-order rate constants using the relation (*25*)

$$\Delta\Delta G_{ij}^{\circ\ddagger}(\text{int}) = -k_B T \ln \Omega_{ij} \quad (5)$$

where the interaction ratio Ω_{ij} is the ratio of rate constants

$$\Omega_{ij} = \frac{k_o(+,-)k_{ij}(-,+)}{k_{ij}(+,+)k_{ij}(-,-)} \quad (6)$$

$k_o(+,-)$ is the second-order rate constant for the reaction between native cyt and native RC and $k_{ij}(-,+)$, $k_{ij}(+,+)$, and $k_{ij}(-,-)$ are the rate constants for reactions in which the charges on residues *i* and *j* are reversed, both being positive or both being negative. For the case in which the two mutation sites are noninteracting, the change in the free energy for the double mutant would be equal to the sum of the change in the free energy due to the single mutants, i.e., $\Delta\Delta G_{ij}^{\circ\ddagger}(\text{int}) = 0$.

The utility of determining $\Delta\Delta G_{ij}^{\circ\ddagger}$(int) is that for simple cases it reflects the specific interaction between mutated residues *i* and *j* (*24*). Thus, it may be used to identify specific interactions that are important in the transition state. The simplest case is where only electrostatic interactions are considered and the structure of the complex is the same in the native and mutant states shown in Figure 2. In this case, the interaction energy is 4 times greater than the Coulomb energy between charges on residues *i* and *j* in the native transition state

$$\Delta\Delta G_{ij}^{\circ\ddagger}(\text{int}) = -4\frac{e^2}{\epsilon r_{ij}^{\ddagger}} \quad (7)$$

where *e* is the electronic charge, ϵ the dielectric constant, and $r_{ij}^{\ddagger}$ the distance between the charges on mutated residues *i* and *j* in the transition state. The origin of the factor of 4 can be seen by calculating $\Delta\Delta G_{ij}^{\circ\ddagger}$(int) from eq 4 for the case where there are only two charges, a positive charge on the cyt and a negative charge on the RC. In that case, $\Delta\Delta G_{ij}^{\circ\ddagger}(-,+) = 0$ and $\Delta\Delta G_{ij}^{\circ\ddagger}(+,+) = \Delta\Delta G_{ij}^{\circ\ddagger}(-,-) = 2e^2/\epsilon r_{ij}^{\ddagger}$. For the case where there are many other charged residues on the cyt and RC, the situation is more complicated due to interactions between mutated residues and other charged residues. However, eq 7 is still applicable due to cancellation of these interaction terms if the distances between charges do not change upon mutation (*24*). More complicated cases can arise if there are changes in the structure of the transition state complex due to mutations. In this study, we assume that $\Delta\Delta G_{ij}^{\circ\ddagger}$(int) is dominated by the Coulomb interaction between mutated residues in the transition state and that the average interaction energy should be inversely proportional to the distance between charges on the mutated residues at the transition state; i.e., large negative interaction energies indicate short distances.

Modeling of the Structure of Cyt−RC Complexes. The X-ray crystal structure of the cocrystal of cyt c_2 and the RC from *Rb. sphaeroides* was used as the basis for modeling the structure of the cyt−RC complex. The structure of the cytochrome c_2 from *Rb. sphaeroides* (*35*) was replaced with the structure of cyt c_2 from *Rb. capsulatus* (*36*) using a least-squares minimization routine to create a hypothetical complex. The structures of cyt c_2 from *Rb. sphaeroides* and *Rb.*

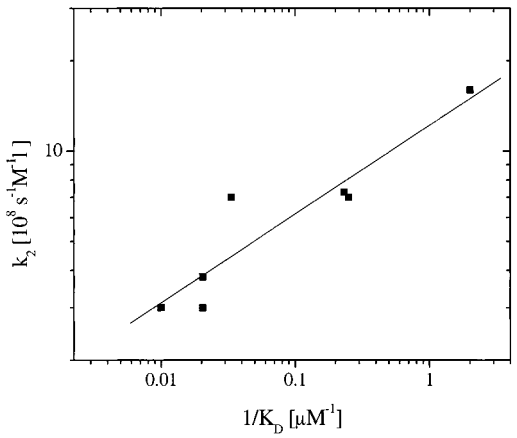

FIGURE 3: Plot of log k_2 vs log $1/K_D$ for the reaction between cyt from *Rb. capsulatus* and the RC from *Rb. sphaeroides*. The slope of the plot ($\alpha = 0.3 \pm 0.05$) relates the changes in transition state energy to the changes in binding energy. The value for α is close to the value found for the reaction between the RC and *Rb. sphaeroides* cyt c_2 (*9*).

capsulatus are very similar (see panels a and b of Figure 1). Thus, it is assumed that they dock in a similar manner. The distances r_{ij} between charges on each of the mutated residues in the model complex were measured. In addition, distances between charged residues in other configurations were obtained by rotating the cyt structure around an axis centered at the contact point between the heme edge, at the CBC methyl group and Tyr L162. In the rotational study, the distances between the relatively fixed positions of the β-carbon atoms of the mutated residues were calculated instead of the distances between charged atoms.

RESULTS

Comparison of K_D and k_2 between Cyt c_2 from Rb. sphaeroides and Cyt c_2 from Rb. capsulatus. The second-order rate constants, k_2, and dissociation constants, K_D, were measured for the reaction of cyt c_2 from *Rb. capsulatus* with modified RCs from *Rb. sphaeroides* having acidic residues replaced with Lys (see Table 1). The values for K_D and k_2 for cyt from the two species are similar (within a factor of 3), showing that the two cytochromes are functionally similar. The values of k_2 for both cytochromes were found to increase with decreasing K_D; i.e., a faster rate constant accompanies stronger binding (see Table 1). A plot of the second-order rate constant k_2 versus $1/K_D$ for cyt c_2 from *Rb. capsulatus* and the RC from *Rb. sphaeroides* is shown in Figure 3. The slope of the plot ($\alpha = 0.30 \pm 0.05$) is similar to the value ($\alpha = 0.4 \pm 0.06$) found using cyt c_2 from *Rb. sphaeroides* (*9*).

Second-Order Rate Constants. Second-order rate constants were measured at low ionic strengths for all combinations of a native and mutant RC from *Rb. sphaeroides* and cyt c_2 from *Rb. capsulatus*. Table 2 shows the matrix of all the measured rate constants for cyt c_2 and the RC. The first row contains k_2 values for reactions between the native RC and mutant cyt c_2. The first column contains k_2 values for reactions between native cyt and mutant RCs. The submatrix, excluding the first column and first row, contains the rate constants for the 30 combinations of six mutant RCs and five mutant cyt c_2.

The rate constants for the reaction between mutant cyt with Lys → Glu replacements and native RCs (top row) were decreased by factors of 5−70-fold. The largest change was produced by the mutation of Lys C99 to Glu. The rate constants for reactions between mutant RCs with Asp/Glu → Lys replacements with native cyt (first column) showed decreases in rate by factors of 2−5. The largest changes were due to mutation of Asp M184 to Lys and Asp L261 to Lys.

Table 2: Second-Order Electron Transfer Rate Constants ($\times 10^6$ M^{-1} s^{-1}) for RCs from *Rb. sphaeroides* and Cyt c_2 from *Rb. capsulatus* Having Charge-Reversing Mutations of Residues in the Interaction Region[a]

	native cyt	KE (C8)	KE (C32)	KE (C54)	KE (C93)	KE (C99)
native RC	1600	330	400	130	79	23
DK (L257)	700	77	200	150	50	2.9
EK (M95)	380	20	51	11	20	46
DK (L155)	730	87	300	170	70	3.6
DK (M292)	700	170	80	7.1	4.6	24
DK (L261)	300	13	57	130	45	0.8
DK (M184)	300	5.9	20	11	18	57

[a] Each entry represents the rate constant for reaction between the species shown by the row and column labels. The underlined rates show compensation, i.e., faster reaction between the mutant cyt and the mutant RC than between the mutant cyt with the native RC. The experimental error is ±15% unless otherwise stated.

The compensatory effects of the cyt mutations on the RC mutations can be seen by reading down the columns that show the reaction of charge-modified cyt with the charge-modified RC. For several double mutant reactions, the rate constants are larger or unchanged compared to the rate of the reaction between mutant cyt and the native RC (underlined in Table 2). These reactions are between cyt mutants modified at Lys C54 [KE (C54)] with RC mutants modified at Asp L257 [DK (L257)], Asp L155 [DK (L155)], and Asp L261 [DK (L261)] and cyt mutants modified at Lys C99 [KE (C99)] with RC mutants modified at Glu M95 [EK (M95)], Asp M292 [DK (M292)], and Asp M184 [DK (M184)] on the RC. These faster rates are indicative of charge compensating interactions between these residues in the cyt−RC complex.

Interaction Energies. The values of $\Delta\Delta G_{ij}^{\circ\ddagger}$(int) calculated from the second-order rate constants using eqs 5 and 6 are shown in Table 3. The values for the strong interactions are underlined. The strongest interaction, i.e., the most negative value of $\Delta\Delta G_{ij}^{\circ\ddagger}$(int), is found between Lys C99 and Asp M184. Strong interactions are also found for Lys C99 with Glu M95 and Asp M292 as well as for Lys C54 with Asp L261, Asp L155, and Asp L257 and between Lys C93 and Asp L261. For purposes of comparison, the distances between charges on residues obtained from the cocrystal structure in the final state are shown in parentheses. In general, there is a correlation between large negative values for $\Delta\Delta G_{ij}^{\circ\ddagger}$(int) and short distances r_{ij} between residues in the cocrystal complex.

Correlation between the Interaction Energy, $\Delta\Delta G_{ij}^{\circ\ddagger}$(int) and Distances in the Cyt−RC Complex. To determine whether the transition state resembles the final bound state of the complex, the interactions obtained from the double mutant analysis were plotted versus the distances obtained from the structure of the cyt−RC complex determined from X-ray crystallography (Figure 4). Despite the relatively large

Table 3: $\Delta\Delta G_{ij}^{\circ\ddagger}$(int) Values,[a] Distances[b] (parentheses), and Correlation Coefficients[c] for Reactions between Mutated RCs from *Rb. sphaeroides* and Mutated Cyt c_2 from *Rb. capsulatus*

	KE (C8)	KE (C32)	KE (C54)	KE (C93)	KE (C99)	correlation coefficient[c] R
DK (L257)	0.63 (39)	−0.13 (23)	−0.97 (6)	−0.37 (7)	1.24 (19)	−0.76
EK (M95)	1.37 (29)	0.62 (32)	1.03 (20)	−0.06 (18)	−2.13 (9)	−0.93
DK (L155)	0.55 (24)	−0.50 (12)	−1.05 (23)	−0.66 (26)	1.07 (25)	−0.32
DK (M292)	−0.16 (10)	0.78 (24)	2.09 (29)	1.93 (31)	−0.87 (22)	−0.54
DK (L261)	1.56 (37)	0.27 (24)	−1.67 (4)	−1.11 (1)	1.68 (14)	−0.90
DK (M184)	2.35 (30)	1.32 (25)	0.80 (12)	−0.19 (11)	−2.58 (7)	−0.96
correlation coefficient[c] R	−0.68	−0.70	−0.70	−0.60	−0.78	

[a] Calculated from data in Table 1 in units of k_BT, i.e., $\ln \Omega_{ij} = -\Delta\Delta G_{ij}^{\circ\ddagger}(\text{int})/k_BT$. The error due to uncertainty in k_2 is $0.4k_BT$. The entries showing strong interactions are underlined. [b] The distances in angstroms, shown in parentheses, were calculated from the structure of the co-crystal of cyt c_2 from *Rb. sphaeroides* and the RC from *Rb. sphaeroides* after replacing the *Rb. sphaeroides* cyt c_2 with coordinates for the cyt c_2 from *Rb. capsulatus*. [c] Correlation coefficients for $\Delta\Delta G_{ij}^{\circ\ddagger}$(int) vs $1/r_{ij}$ calculated for the individual residues (single rows or columns) (*37*). The high correlation coefficients (close to 1) for Asp M184, Glu M95, and Asp L261 indicate the importance of these residues in orienting the cyt for electron transfer.

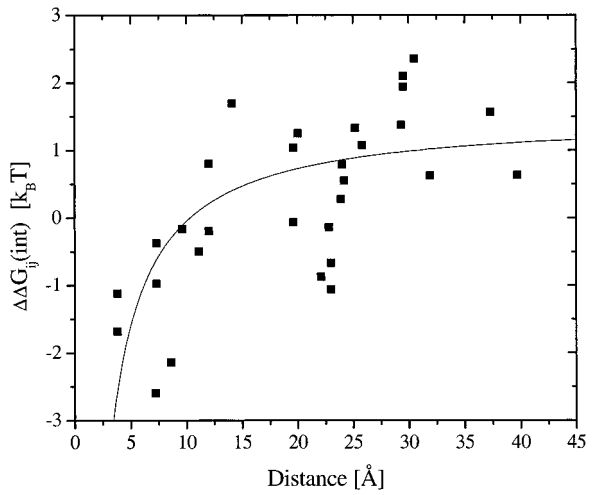

FIGURE 4: Plot of $\Delta\Delta G_{ij}^{\circ\ddagger}(\text{int})/k_BT$ vs r_{ij} for the reaction between cyt and the RC. The values of $\Delta\Delta G_{ij}^{\circ\ddagger}(\text{int})/k_BT = -\ln \Omega_{ij}$ (in units of k_BT, i.e., eq 5) were obtained from the second-order rate constants for reactions between cyt and the RC having mutations of charged residues *i* and *j*. The values of r_{ij} are the measured distances between the residues in the X-ray crystal structure of the cyt−RC complex. The large spread in the data is due to fluctuations in the average distance between charges in the transition state. The line is the function $a/r_{ij} + b$ ($a = -15$ Å $\times$ k_BT and $b = 1.5k_BT$).

scatter in the data, the result shows a correlation consistent with a $-1/r_{ij}$ dependence, i.e., decreasing values of $\Delta\Delta G_{ij}^{\circ\ddagger}$(int) with decreasing r_{ij}. The data in Figure 4 were fit with a function $\Delta\Delta G_{ij}^{\circ\ddagger}(\text{int}) = a/r_{ij} + b$, where $a = -15$ Å(k_BT) and $b = 1.5k_BT$. The positive value of b suggests that an unfavorable interaction arises when two mutations are present in the cyt−RC complex.

A statistical test of the dependence of $\Delta\Delta G_{ij}^{\circ\ddagger}$(int) versus $1/r_{ij}$ was made by calculating the linear correlation coefficient, R, for the two variables using the distances obtained from the cocrystal structure. The linear correlation coefficient is a statistical parameter that tests whether a linear functional relationship exists between two quantities (*37*). R has values ranging from −1 to 1. A correlation coefficient of −1 would be expected for data with an exact linear dependence between $\Delta\Delta G_{ij}^{\circ\ddagger}$(int) and $1/r_{ij}$. A correlation coefficient of −0.63 was found between $\Delta\Delta G_{ij}^{\circ\ddagger}$(int) and the $1/r_{ij}$ values for interactions between all mutated residues. This indicates that a significant correlation exists.

A correlation test was also performed for the data from individual amino acid residues. Strong correlations were found for interactions of Asp M184, Glu M95, and Asp L261 with R values of −0.96, −0.93, and −0.90, respectively (see Table 3). The high correlation for these acidic groups would arise if the position of the charges on the cyt were relatively fixed relative to these groups in the transition state. This would be the case if the positions of these residues relative to the cyt were important for the transition state. Thus, the strong correlation suggests that Asp M184, Glu M95, and Asp L261 play important roles in orienting the cyt on the RC surface.

Comparison with Other Structural Models. To test whether the correlation between $\Delta\Delta G_{ij}^{\circ\ddagger}$(int) and $1/r_{ij}$ was significant, other structural models were tested to see how well they could account for the experimental data. A series of models were constructed by rotating the cyt around an axis consisting of the contact point of the heme edge with Tyr L162. In this test, the distances from the β-carbon atoms were used instead of the distances between charges, to approximate the average distance between charges. The linear correlation coefficient, R, for the variables $\Delta\Delta G_{ij}^{\circ\ddagger}$(int) and $1/r_{ij}$ was calculated. A plot of the value of $-R$ versus angle, shown in Figure 5, has a peak near 0°. Since the structure at 0° is the cocrystal structure, this peak indicates that the cocrystal structure matches the pattern of distances between charged residues in the transition state. This supports the idea that the orientation of the cyt on the RC surface in the transition state is similar to that of the complex in the cocrystal.

DISCUSSION

In this study, we have addressed the question of the specific electrostatic interactions at the interface of the complex between the cyt c_2 from *Rb. capsulatus* and the RC from *Rb. sphaeroides* by looking for the effects of compensating mutations on the RC and cyt. Changes in the second-order rate constant, k_2, were observed and used to calculate an interaction energy $\Delta\Delta G_{ij}^{\circ\ddagger}$(int) which is related to the interaction between charges on the mutated residues. The main findings are as follows: (1) The association process is dominated by a few major interactions. (2) Strong interaction energies in the transition state are correlated with short distances between residues in the co-crystal complex in the

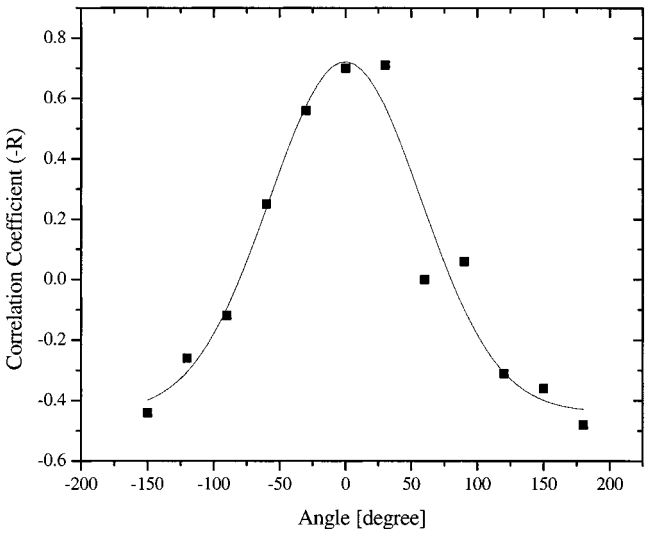

FIGURE 5: Plot of the correlation coefficient $-R$ vs the angle θ for different models of the cyt−RC complex. The cyt was rotated on the surface of the RC around an axis centered at the contact between the heme edge and Tyr L162. The correlation coefficients between $\Delta\Delta G_{ij}^{\circ\ddagger}$(int) and $1/r_{ij}$ were calculated using the values for $\Delta\Delta G_{ij}^{\circ\ddagger}$(int) and the measured values of r_{ij} from the different structures. The solid line is a Gaussian function fit to the data. The fit of the correlation coefficient data has a peak near $\theta = 0$, indicating that the orientation of the cyt in the transition state is similar to that of the final state of the complex.

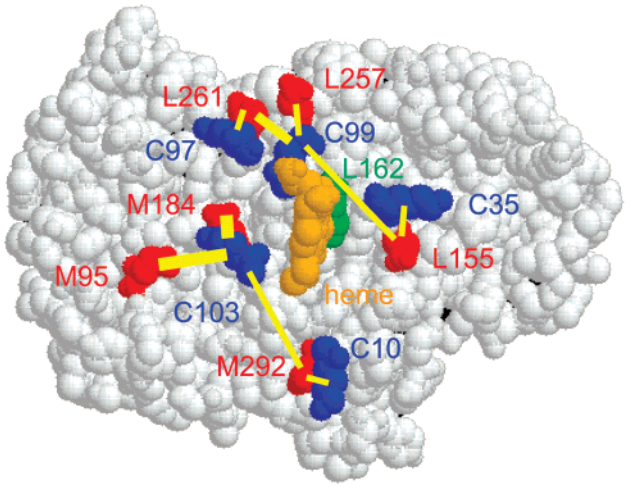

FIGURE 6: Surface view of the contact region of the X-ray crystal structure of the cyt−RC complex from *Rb. sphaeroides* showing the positions of the mutated charged residues and electron transfer contact groups (*21*). The color code is as follows: charged residues such as Lys (blue), acidic residues (red), electron tunneling contact groups such as heme (orange), and Tyr L162 (green). Yellow lines are drawn between strongly interacting residues. The widths of the lines are proportional to $\Delta\Delta G_{ij}^{\circ\ddagger}$(int) $- b$, indicating the strength of the interactions between the residues in the transition state. Note that distances are larger than they appear here in projection.

final state (Figures 4 and 5). This correlation supports the proposal (*9*) that the transition state resembles the final state.

Spatial Distribution of Interactions between Charged Residues in the Cyt−RC Complex. The spatial distribution of the electrostatic interactions between the mutated residues, obtained from the interaction energy, $\Delta\Delta G_{ij}^{\circ\ddagger}$(int), is displayed graphically in Figure 6. This figure shows the positions of the mutated Lys residues (blue) from the cyt and the mutated carboxylic acid residues (red) in a view of the periplasmic surface of the RC from the X-ray structure of the cyt−RC complex from *Rb. sphaeroides* (*21*). In this structure, the heme (orange) is positioned over the tunneling contact point, Tyr L162 (green), directly over the bacteriochlorophyll dimer. The strong interactions obtained from the double mutant analysis are shown by yellow lines between mutated residues. The widths of the lines are proportional to $\Delta\Delta G_{ij}^{\circ\ddagger}$(int) $- b$ (where b is an offset parameter determined experimentally; see Figure 4) to show the strength of the electrostatic interaction between the residues. The strongest interactions are between Lys C99 and a cluster of acidic residues (Asp M184, Glu M95, and Asp M292) that surround this Lys in the cocrystal structure. The second largest interactions are due to Lys C54 and a cluster of acidic residues (Asp L261, Asp L257, and Asp L155) that surround the Lys residue in the cocrystal structure. Interactions between Lys C93 and Asp L261, between Lys C32 and Asp L155, and between Lys C8 and Asp M292 are observed between residues in proximity in the crystal structure. In most cases, the strongest interaction is found between residues that are closest together in the crystal structure (Table 3). Two exceptions are the relatively small interactions of Asp M292 and Asp L155 with their closest Lys partners in the cocrystal, Lys C8 and Lys C32, respectively. Instead, Asp M292 and Asp L155 have their largest interactions with Lys C99 and Lys C54, respectively, despite relatively long distances between these residues in the cocrystal (Table 3). The strong interactions of Lys C99 and Lys C54 with Asp M292 and Asp L155, respectively, and other residues near their docking sites near Asp M184 and Asp L261, respectively (see Figure 6), suggest that these interactions play a dominant role in the transition state.

Docking Interactions in the Cyt−RC Complex. The study of charge compensating mutations on the RC and cyt provides insight into the energetics and dynamics of the protein association process for the formation of the active cyt−RC complex. The single mutant results of modified RCs with native cyt c_2 from *Rb. capsulatus* show the key role of Asp M184 and Asp L261 (Table 2). This is in agreement with the earlier mutant studies that showed large changes in K_D and k_2 due to changes in these residues in reaction with cyt c_2 from *Rb. sphaeroides* (*9*, *18*). The single mutant results of modified *Rb. capsulatus* cyt c_2 show the key roles of Lys C99, Lys C93, and Lys C54 (Table 2). The changes due to cyt mutations are larger than those from RC mutations (Table 2). The origin of this asymmetry is not understood at present but may be related to steric interference from cyt mutations that inhibit binding or electron transfer and to interactions of Lys residues with several acidic residues from the RC in the transition state (see Figure 6).

The interactions from the double mutant study give information about the specific interactions that are important for docking. The dominant interaction is between Lys C99 and the cluster of acidic residues around Asp M184 (see Figure 6). The Asp M184 region represents the most negative potential energy region on the RC (*9*), and it is reasonable that this should be a "hot spot". However, the choice of C99 as a partner is not as easily understood, since C99 is relatively undistinguished on the potential surface of the cyt (*9*). One possible factor is the short distance between Lys C99 and Phe C98. The corresponding Phe (S102 in *Rb. sphaeroides*) is in van der Waals contact with hydrophobic residues Leu

M191 and Val M192 near Tyr L162 in the cocrystal structure. The association of Lys C99 with Asp M184 may bring Phe 98 in close contact with these hydrophobic residues to nucleate the formation of short-range interactions that position the heme edge close to Tyr L162.

On the basis of the interactions found from this study and the crystal structure of the cocrystal, we propose a cyt docking mechanism that includes the specific interactions found in this work. The first step in docking involves the orientation of cyt and the RC due to long-range nonspecific interactions between complementary charges on the cyt and RC to form a loose encounter complex lacking specific charge interactions (*11*, *19*, *38*). After the encounter complex is formed and the two proteins are brought into closer contact, the specific interaction of Lys C99 at the region of strong negative potential near the Asp M184 and Asp M95 site brings these regions into juxtaposition. As the cyt more closely approaches the RC, the weaker interaction between Lys C54 and the region of negative potential near Asp L257 and Asp L261 comes into effect, guiding the cyt into position on the RC surface. At this point, short-range interactions between groups on the cyt and RC could help stabilize the cyt in the active position on the RC surface. The active position is proposed to be a conformation (or range of conformations) close to that found in the co-crystal structure (*21*). Hydrophobic interactions between Phe C98 on the cyt and hydrophobic residues Leu M191 and Val M192 on the RC, as well as a $\pi-$cation interaction between Arg C32 and Tyr M295 seen in the cocrystal, could help fix the cyt on the RC surface with close contact between redox cofactors for fast electron transfer. In the cocrystal structure, the heme CBC methyl group is in close contact with Tyr L162 on the RC. The distance between the CBC methyl group on the heme and the ring ethyl group from $BChl_2$ is 8.4 Å. This short distance facilitates electron tunneling from the heme to the Bchl dimer (*39*).

The proposed scenario for docking involves different interactions at different length scales and thus time scales; i.e., long-range interactions occur before short-range interactions, giving rise to a temporal order for the sequence of events. The effect of these interactions could act like a "funnel", directing configurations of the cyt relative to the RC into the active configuration, conceptually similar to a protein-folding funnel (*40*). The funneling effect would result in the efficient docking of the cyt onto the RC for electron transfer.

Two questions arise in comparing the sequence of steps proposed above with the reactions shown in eq 2. (1) What is the structure of the transition state $(cyt^{2+}-RC)^{\ddagger}$? The results from this study indicate that specific long-range electrostatic interactions, most notably, between Lys C99 and Lys C54 on the cyt and negatively charged partners on the RC, are formed at the transition state. However, we do not know if short-range hydrophobic or cation$-\pi$ interactions are also present at the transition state or if they are formed at a later stage in the reaction as the transition state complex collapses on its way to the final state. (2) What is the structure of the state active in electron transfer, $(cyt^{2+}-RC)^*$? The similarity between the transition state and the co-crystal structure that is likely to be optimized for electron transfer with a close juxtaposition of the heme edge and Tyr L162 at the tunneling interface suggests that the state that is active in electron transfer, $(cyt^{2+}-RC)^*$, has the structure of the thermodynamically stable final state. This is likely to be the case if the rate of relaxation from the transition state to the stable state is fast compared to the rate of electron transfer. The findings from this work thus indicate that the cyt−RC complex is optimized for binding and electron transfer, a very reasonable design feature. However, it should be noted that this is not always the case (see ref *41*). To test the proposed mechanism, more information about the distance dependence of electron transfer and the dynamics of protein association must be obtained.

Double Mutant Analysis. The double mutant analysis provides a powerful means of detecting interactions that are important for protein−protein association. This method can be used qualitatively to identify residues that interact in the transition state preceding the formation of the complex involved in electron transfer. In addition, we use some quantitative arguments to correlate the observed rates to distances between charges in the transition state.

Several simplifying assumptions were made in the analysis. The first assumption is that the interaction is dominated by electrostatic effects. The justification for this comes from the low value of α (0.3−0.4), indicating that the interactions in the transition state are weak which suggests a transition state complex in which charged residues are relatively far apart [e.g., >10 Å (*9*)]. In addition, the structure of the cyt−RC complex shows relatively long (6−10 Å) distances between charged residues in the interface region and an absence of specific salt-bridged interactions. Thus, long-range electrostatic interactions are likely to dominate. The second assumption is that the single and double mutant complexes have the same structure. This assumption is unlikely to be strictly correct since the changes in electrostatic interactions can alter the structure in the interface region and the sizes of the amino acid side chains are changed due to mutation.

The change in structure of the transition state due to mutations is likely to be the largest source of error. However, since the overall interaction arises from many charged residues, the mutation of one charge may not greatly change the structure of the complex. Another source of error is the difference between cyt c_2 from *Rb. capsulatus* and *Rb. sphaeroides*, although the good agreement between the interactions found here and the structure of the cocrystal complex would suggest that the similarities are more important than the differences. Some of the errors that arise in correlating the interaction energy to distance between charges could have been avoided if mutations to neutral residues were studied. In that case, the interaction energy would be equal to the Coulomb energy in the native state, assuming again no changes in structure. Thus, the advantage of the charge-reversing mutations used in this study is that the interaction energy is increased by as much as a factor of 4. This increase in the size of the measured effect facilitates detection. For instance, a factor of 4 reduction in $\Delta\Delta G_{ij}^{\circ\ddagger}$(int) would decrease the largest interaction ratio (Ω) found in this study (between Lys C99 and Asp M184) from 13 to 2, making it more difficult to measure accurately.

Concluding Remarks. The effect of compensating charge mutations on the rates of intermolecular electron transfer has been used to identify specific electrostatic interactions that are responsible for protein association. Strong interactions are found between residues that are close to each other in

the cocrystal cyt−RC complex, indicating that the structure of the transition state in solution is similar to the structure of the final state of the complex in the crystalline state. The strong interaction between Lys C99 on the cyt with the cluster of negatively charged residues near Asp M184 on the RC suggests a key role for these residues in the association process. These tentative conclusions could be checked by further double (and triple) mutant studies, including charge neutralizing mutations and mutations to cyt c_2 from *Rb. sphaeroides*. In any case, the studies reported here provide the basis for a detailed molecular picture of the dynamics of docking and electron transfer.

ACKNOWLEDGMENT

We thank Andrea Juth, Trieva Turanchick, Heather Mekosh, and John Fitch for technical assistance and George Feher, Mark Paddock, and Jose Onuchic for helpful discussions.

REFERENCES

1. Bendall, D., Ed. (1996) *Protein Electron Transfer*, Bios Scientific Publishers Ltd., Oxford, U.K.
2. Feher, G., Allen, J. P., Okamura, M. Y., and Rees, D. C. (1989) *Nature 339*, 111−116.
3. Tiede, D., and Dutton, P. (1993) in *The Photosynthetic Reaction Center* (Deisenhofer, J., and Norris, J., Eds.) pp 258−288, Academic Press, San Diego.
4. Prince, R. C., Cogdell, R. J., and Crofts, A. R. (1974) *Biochim. Biophys. Acta 347*, 1−13.
5. Overfield, R. E., Wraight, C. A., and Devault, D. C. (1979) *FEBS Lett. 105*, 137−142.
6. Rickle, G., and Cusanovich, M. (1979) *Arch. Biochem. Biophys. 197*, 589−598.
7. Moser, C., and Dutton, P. L. (1988) *Biochemistry 27*, 2450−2461.
8. Venturoli, G., Drepper, F., Williams, J., Allen, J., Lin, X., and Mathis, P. (1998) *Biophys. J. 74*, 3226−3240.
9. Tetreault, M., Rongey, S. H., Feher, G., and Okamura, M. (2001) *Biochemistry 40*, 8452−8462.
10. Lin, X., Williams, J. C., Allen, J., and Mathis, P. (1994) *Biochemistry 33*, 13517−13523.
11. Caffrey, M. S., Bartsch, R. G., and Cusanovich, M. A. (1992) *J. Biol. Chem. 267*, 6317−6321.
12. Tiede, D. M., and Vashista, A.-C. J. (1991) *Mol. Cryst. Liq. Cryst. 184*, 191−200.
13. Long, J., Durham, B., Okamura, M., and Millett, F. (1989) *Biochemistry 28*, 6970−6974.
14. Rosen, D., Okamura, M. Y., Abresch, E. C., Valkirs, G. E., and Feher, G. (1983) *Biochemistry 22*, 335.
15. Drepper, F., Dorlet, P., and Mathis, P. (1997) *Biochemistry 36*, 1418−1427.
16. Tiede, D. M., and Chang, C.-H. (1988) *Isr. J. Chem. 28*, 183−191.
17. Allen, J. P., Feher, G., Yeates, T. O., Komiya, H., and Rees, D. C. (1987) *Proc. Natl. Acad. Sci. U.S.A. 84*, 6162−6166.
18. Adir, N., Axelrod, H., Beroza, P., Isaacson, R., Rongey, S., Okamura, M., and Feher, G. (1996) *Biochemistry 35*, 2535−2547.
19. Tiede, D., Vashishta, A., and Gunner, M. (1993) *Biochemistry 32*, 4515−4531.
20. Tiede, D. (1987) *Biochemistry 26*, 397−410.
21. Axelrod, H. L., Abresch, E. C., Okamura, M. Y., Yeh, A. P., Rees, D. C., and Feher, G. (2002) *J. Mol. Biol.* (in press).
22. Wachtveitl, J., Farchaus, J., Mathis, P., and Oesterhelt, D. (1993) *Biochemistry 32*, 10894−10904.
23. Dohse, B., Mathis, P., Wachtveitl, J., Laussermair, E., Iwata, S., Michel, H., and Oesterhelt, D. (1995) *Biochemistry 34*, 11335−11343.
24. Serrano, L., Horovitz, A., Avron, B., Bycroft, M., and Fersht, A. (1990) *Biochemistry 29*, 9343−9352.
25. Hidalgo, P., and MacKinnon, R. (1995) *Science 268*, 307−310.
26. Schreiber, G., and Fersht, A. (1995) *J. Mol. Biol. 248*, 478−486.
27. Gong, X., Wen, J., Fisher, N., Young, S., Howe, C., Bendall, D., and Gray, J. (2000) *Eur. J. Biochem. 267*, 3461−3468.
28. Guillouard, I., Lagoutte, B., Gwneaelle, M., and Bottin, H. (2000) *Biochem. Biophys. Res. Commun. 271*, 647−653.
29. Tetreault, M., Cusanovich, M., Meyer, T., Feher, G., and Okamura, M. Y. (1999) *Biophys. J. 76*, A20.
30. Daldal, F., Cheng, S., Applebaum, J., Davidson, E., and Prince, R. (1986) *Proc. Natl. Acad. Sci. U.S.A. 83*, 2012−2016.
31. Keen, N., Tamaki, S., Kobayashi, D., and Trollinger, D. (1988) *Gene 70*, 191−197.
32. Wall, J. D., Weaver, P. F., and Gest, H. (1975) *Arch. Microbiol. 105*, 217−224.
33. Bartsch, R. (1978) in *The Photosynthetic Bacteria* (Clayton, R., and Sistrom, W., Eds.) pp 249−279, Plenum Press, New York.
34. Paddock, M. L., Rongey, S. H., Feher, G., and Okamura, M. Y. (1989) *Proc. Natl. Acad. Sci. U.S.A. 86*, 6602−6606.
35. Axelrod, H., Feher, G., Allen, J., Chirino, A., Day, M., Hsu, B., and Rees, D. (1994) *Acta Crystallogr. D50*, 596−602.
36. Benning, M., Wesenberg, G., Caffrey, M., Bartsch, R., Meyer, T., Cusanovich, M., Rayment, I., and Holden, H. (1991) *J. Mol. Biol. 220*, 673−685.
37. Bevington, P. R. (1969) *Data Reduction and Error Analysis for the Physical Sciences*, McGraw-Hill, New York.
38. Koppenol, W., and Margoliash, E. (1982) *J. Biol. Chem. 257*, 4426−4437.
39. Aquino, A., Beroza, P., Beretan, D., and Onuchic, J. (1995) *Chem. Phys. 197*, 277−288.
40. Leopold, P., Montal, M., and Onuchic, J. (1992) *Proc. Natl. Acad. Sci. U.S.A. 89*, 8721−8725.
41. Meyer, T., Zhao, Z., Cusanovich, M., and Tollin, G. (1993) *Biochemistry 32*, 4552−4559.

BI012053E